Missouri University of Science and Technology
Scholars' Mine

Physics Faculty Research & Creative Works | Physics

01 Sep 2019

A Dynamical (e,2e) Investigation into the Ionization of the Outermost Orbitals of R-Carvone

D. B. Jones

E. Ali

C. G. Ning

F. Ferreira Da Silva

et. al. For a complete list of authors, see https://scholarsmine.mst.edu/phys_facwork/2058

Follow this and additional works at: https://scholarsmine.mst.edu/phys_facwork

 Part of the Physics Commons

Recommended Citation

D. B. Jones et al., "A Dynamical (e,2e) Investigation into the Ionization of the Outermost Orbitals of R-Carvone," *Journal of Chemical Physics*, vol. 151, no. 12, American Institute of Physics (AIP), Sep 2019. The definitive version is available at https://doi.org/10.1063/1.5123526

This Article - Journal is brought to you for free and open access by Scholars' Mine. It has been accepted for inclusion in Physics Faculty Research & Creative Works by an authorized administrator of Scholars' Mine. This work is protected by U. S. Copyright Law. Unauthorized use including reproduction for redistribution requires the permission of the copyright holder. For more information, please contact scholarsmine@mst.edu.

The Journal of Chemical Physics ARTICLE scitation.org/journal/jcp

A dynamical (e,2e) investigation into the ionization of the outermost orbitals of *R*-carvone

Cite as: J. Chem. Phys. 151, 124306 (2019); doi: 10.1063/1.5123526
Submitted: 6 August 2019 • Accepted: 31 August 2019 •
Published Online: 26 September 2019

View Online Export Citation CrossMark

D. B. Jones,[1,a] E. Ali,[2] C. G. Ning,[3] F. Ferreira da Silva,[4] O. Ingólfsson,[5] M. C. A. Lopes,[6] H. S. Chakraborty,[2] D. H. Madison,[7] and M. J. Brunger[1]

AFFILIATIONS

[1]College of Science and Engineering, Flinders University, GPO Box 2100, Adelaide, SA 5001, Australia
[2]Department of Natural Sciences, D. L. Hubbard Center for Innovation, Northwest Missouri State University, Maryville, Missouri 64468, USA
[3]State Key Laboratory of Low-Dimensional Quantum Physics, Department of Physics, Tsinghua University, Beijing 100084, China
[4]Atomic and Molecular Collisions Laboratory, CEFITEC, Department of Physics, Universidade NOVA de Lisboa, 2829-516 Caparica, Portugal
[5]Department of Chemistry and Science Institute, University of Iceland, 107 Reykjavík, Iceland
[6]Departamento de Física, Universidade Federal de Juiz de Fora, Juiz de Fora, MG 36036-900, Brazil
[7]Department of Physics, Missouri University of Science and Technology, Rolla, Missouri 65409, USA

[a]**Author to whom correspondence should be addressed:** darryl.jones@flinders.edu.au

ABSTRACT

We report an experimental and theoretical investigation into the dynamics of electron-impact ionization of *R*-carvone. Experimental triple differential cross sections are obtained in asymmetric coplanar kinematic conditions for the ionization of the unresolved combination of the three outermost molecular orbitals (41a-39a) of *R*-carvone. These cross sections are compared with theoretical cross sections calculated within a molecular 3-body distorted wave (M3DW) framework employing either a proper orientation average or orbital average to account for the random orientation of the molecule probed in the experiment. Here, we observe that the overall scattering behavior observed in the experiment is fairly well reproduced within the M3DW framework when implementing the proper average over orientations. The character of the ionized orbitals also provides some qualitative explanation for the observed scattering behavior. This represents substantial progress when trying to describe the scattering dynamics observed for larger molecules under intermediate-impact energy and asymmetric energy sharing scattering conditions.

Published under license by AIP Publishing. https://doi.org/10.1063/1.5123526

I. INTRODUCTION

Pioneering work has established that DNA strand breakages could occur through dissociative electron attachment processes.[1] This prompted a concerted theoretical and experimental effort to understand electron-interactions with biologically relevant molecules,[2] in order to describe the complete range of scattering phenomena occurring when biological systems are exposed to ionizing radiation. These collisional cross sections have been benchmarked utilizing swarm/transport simulation techniques[3–6] and subsequently incorporated into charged particle transport simulations describing the effects of radiation on tissue and processes within plasma-like environments.[4,5,7–10] This approach, while originally focusing on charged-particle interactions relating to radiation and plasma-medical environments, is also extended to describing industrial and naturally occurring plasma-like environments.[11,12]

One aspect of this work has included investigating the dynamics of the ionization process for large biomolecular targets.[13–16] While significant progress has been made in describing ionization

Published under license by AIP Publishing

of atoms,[17,18] it is still particularly challenging to describe ionization processes for larger molecules. While our investigations have attempted to rectify the paucity of data available relating to electron-impact ionization phenomena for larger molecules, we have also judiciously selected molecular targets in an attempt to understand the role that molecular structure plays in the dynamics of the ionization process. In these targets, we have focused on the ionization of the outermost orbitals, which typically involve nonbonding oxygen atom contributions. These structural changes related to the addition of side chains in going from tetrahydrofuran to tetrahydrofurfuryl alcohol,[15,19,20] modifications to the ring environment in cyclic ethers,[14,21] and oxygen attachments to ring structures in phenol[22] and *para*-benzoquinone.[23]

In the present contribution, we extend our investigations into the ionization dynamics of *R*-carvone ($C_{10}H_{14}O$). *R*-carvone, and its chiral enantiomer (S-carvone), are naturally occurring species that can be extracted from spearmint and caraway seeds [see Fig. 1(a)]. These compounds are important for the flavor and fragrance industry,[24] and they and their derivatives also display significant biological activities. These include central nervous system interactions to stimulate antinociceptive and anti-inflammatory effects,[25] in addition to displaying antimicrobial and antifungal[24] properties. We are particularly interested in studying the ionization dynamics of molecules with known biological activity, as the dynamical ionization process may provide clues for unlocking the structure-activity relationships. Here, in particular, carvone also possesses many of the same key functional groups (ketone) contained by other targets we have investigated.

In this contribution, we consider the dynamics of the electron-impact ionization of the unresolved combination of the three-outermost molecular orbitals (41a-39a) of *R*-carvone. The kinematically complete electron-impact ionization of *R*-carvone can be described through

$$e_0^-(E_0,\boldsymbol{k}_0)+T_{Carvone}\rightarrow T^+_{Carvone}(\epsilon_i,\boldsymbol{q})+e_1^-(E_1,\boldsymbol{k}_1)+e_2^-(E_2,\boldsymbol{k}_2). \quad (1)$$

Here, $e_j^-(E_j,\boldsymbol{k}_j)$ is the jth electron with energy and momentum, E_j and $\boldsymbol{k}_j$, respectively. In addition, the subscripts, j = 0, 1, and 2, refer to the incident, fast scattered, and slow ejected electrons, respectively. Conservation of energy within the collision requires that

$$\epsilon_i = E_0 - (E_1 + E_2), \quad (2)$$

where ϵ_i is the energy required to ionize an electron from the i-th molecular orbital of the carvone target $T_{carvone}$. To conserve momentum, the residual ion ($T^+_{Carvone}$) recoils with momentum

$$\boldsymbol{q} = \boldsymbol{k}_0 - (\boldsymbol{k}_1 + \boldsymbol{k}_2). \quad (3)$$

To study the dynamics of the ionization process, we report triple differential cross sections (TDCS) obtained under asymmetric coplanar kinematic conditions. Here, angular distributions of the slow

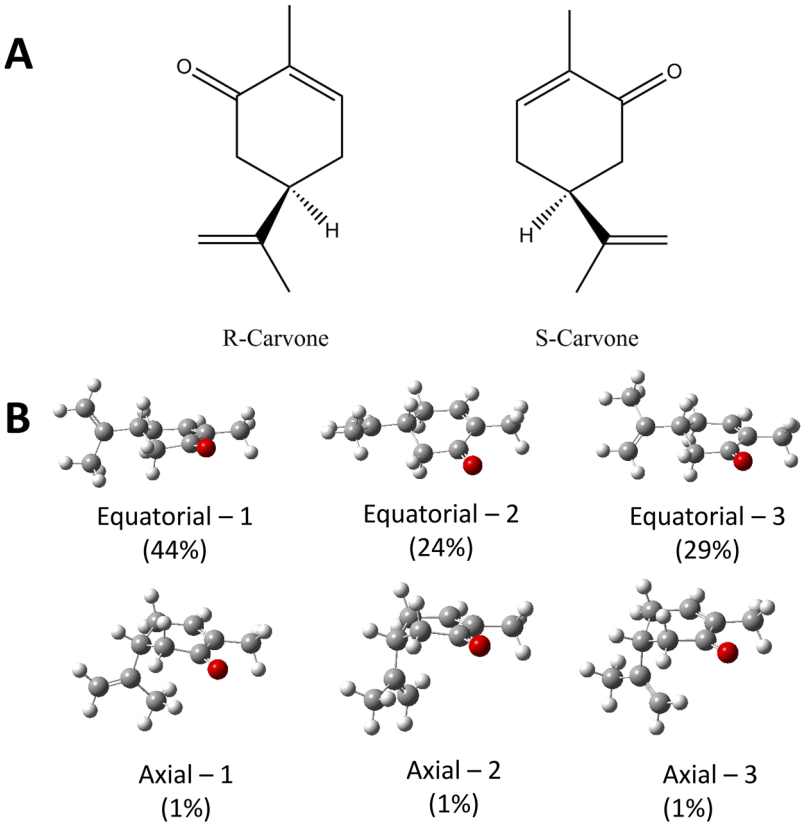

FIG. 1. (a) The molecular structure of *R*-carvone, and its chiral enantiomer, *S*-carvone. (b) The 6-possible conformers of *R*-carvone.

Published under license by AIP Publishing

outgoing electron are reported for the fixed fast-scattered electron angles, $\theta_1 = -5°$, $-10°$, and $-15°$. By fixing the fast electron's scattering angle, the momentum transferred to the target during the collision

$$\boldsymbol{K} = \boldsymbol{k}_0 - \boldsymbol{k}_1 \tag{4}$$

also becomes fixed. Under the present kinematical conditions, the momentum transfer magnitude increases with the changing scattered electron angle from $\theta_1 = -5°$ to $-15°$, ranging from 0.44 to 1.12 a.u., respectively. The momentum transfer magnitude is typically less than or close to that of the slow outgoing electron $|\boldsymbol{K}| \leq |\boldsymbol{k}_2|$. Such conditions are therefore particularly sensitive to the collisional scattering dynamics.

In the discussion of TDCS angular distributions, we often refer to the binary and recoil regions. Under an asymmetric coplanar kinematic condition, the binary region represents the angular region of the TDCS where the ejected electron lies in the direction close to that of the momentum transfer (+K). Here, the incident electron is assumed to have had a binary encounter with the target electron. Likewise, the recoil region is the angular range of the TDCS where the ejected electron is directed into the angular region antiparallel to the momentum transfer direction (−K). For this backscattering to occur, it is anticipated that the electron has also undergone scattering from the nuclei. These conditions are therefore important for bridging our understanding of phenomena occurring between high energy and low energy ionization regimes, and elucidating the role of momentum transfer during the dynamical collision process.

Characterizing the dynamics of the ionization process is important for improving simulations of electron transport in matter. As an example, the low-energy charged particle tracking simulation (LEPTS) code[7,8,26,27] utilizes cross section data to predict charged-particle tracks and energy deposition. Currently, these simulations assume that all secondary electrons produced in ionization events are ejected in the direction of the momentum transfer (+K).[28] This assumption neglects the shape of binary peak features and discounts the possibility of any recoil scattering. It is therefore imperative that theoretical tools are developed, so that an improved physical description of the ionization process can be incorporated into the available charged-particle transport codes including Boltzmann analyses of transport in electron and positron swarms.[29]

The outline of our manuscript is as follows: In Sec. II, we describe our experimental and theoretical methods. This is followed by a presentation and discussion of our results (see Sec. III). Finally, the conclusions from this work are summarized in Sec. IV.

II. EXPERIMENTAL AND THEORETICAL DETAILS

Triple differential cross sections for the electron-impact ionization of *R*-carvone are studied using an (e,2e) experiment, where the energy and momentum of both outgoing electrons are determined in a time-coincidence technique. The experimental apparatus used and details of its operation have been reported previously,[30] and so only a brief description is repeated here.

A liquid sample of *R*-(−)-carvone (98% assay, Sigma-Aldrich) was prepared by degassing through repeated freeze-pump-thaw cycles. This sample was then heated to ~40 °C, with the vapor allowed to flow into the vacuum chamber through a beam forming needle. The operating chamber pressure throughout the experiment was typically $1–2 \times 10^{-6}$ Torr, with the vacuum chamber also being heated to prevent condensation of the carvone vapor. The effusive beam of *R*-carvone is crossed with a fixed energy electron beam. Electrons scattering from the molecular beam are detected using two energy selective analyzers that are mounted on independently rotatable turntables.[30] Carvone was a particularly challenging species to work with, as it was difficult to pump out of the vacuum system and it reduced the lifetime of the electron gun filament.

The binding energy spectrum of carvone (see Fig. 2) was first obtained by recording the number of true coincident counts while scanning over a range of scattered electron detection energies. Here, both the scattered and ejected analyzer angular positions are fixed, being $\theta_1 = -10°$ and $\theta_2 = 75°$, respectively. The incident (E_0 = 250 eV) and ejected (E_2 = 20 eV) electron energies are also fixed, enabling the scattered electron energy to be converted to a binding energy through the conservation of energy [Eq. (2)]. The binding energy spectrum is then used to set the scattered electron energy to match the ionization potential of the binding energy feature corresponding to the unresolved combination of the outermost (41a-39a) molecular orbitals of *R*-carvone for the TDCS angular distribution measurements.

Angular distributions of the triple differential cross section in this study were measurements for the electron-impact ionization of the unresolved combination of the three outermost molecular orbitals of *R*-carvone. Here, the scattered electron energy is set to

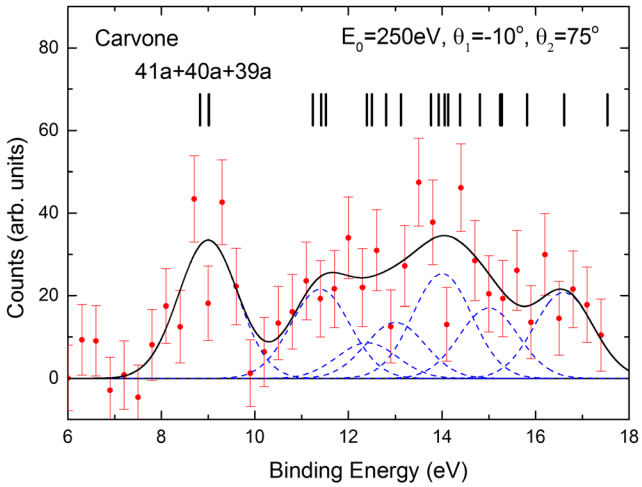

FIG. 2. The measured (e,2e) binding energy spectrum for *R*-carvone. This was obtained at an incident electron energy of E_0 = 250 eV by scanning over a range of detection energies for a fast electron scattered through an angle of −10°. Here, the slow ejected electron was detected with an energy of E_2 = 20 eV and at a scattering angle of 75°. The positions of the OVGF ionization energies for the dominant equatorial (eq-1) conformer are also shown. Also shown are the spectral deconvolution for the resolved orbital features (dashed lines) and their sum (solid line). See text for further details.

Published under license by AIP Publishing

match the peak maximum in the binding energy spectrum for the unresolved outermost feature (41a-39a), while keeping the energies of incident and slow outgoing electrons constant, again at 250 and 20 eV, respectively. Given the energy resolution of our spectrometer (~1.1 eV) and the close-lying nature of those molecular orbital (~0.5 eV), we believe that they are all contributing to the experimental TDCS angular distributions. TDCS angular distributions at fixed fast scattered electron angles are obtained by recording the number of true coincident events observed, while repeatedly scanning over a range of discrete slow ejected electron angles. The obtained angular distributions of the TDCS are then internormalized by recording the TDCS angular distribution for the fast scattered electron, while keeping the detected slow ejected electron angle at a fixed position of 85°.

Triple differential cross sections for the electron impact ionization of carvone were calculated within the molecular three-body distorted wave (M3DW) approximation. The M3DW framework is fully described in previous publications,[31–33] and so only a brief description is repeated here. The M3DW direct scattering transition matrix for a fixed in space molecule, with molecular orientation ($\boldsymbol{R}$), is given by

$$T_{dir}(\boldsymbol{R}) = \langle \chi_1^-(\boldsymbol{k}_1, \boldsymbol{r}_1)\chi_2^-(\boldsymbol{k}_2, \boldsymbol{r}_2)C_{12}(\boldsymbol{r}_{12}) \times |V_0 - U_0|\phi_{Dy}(\boldsymbol{r}_2, \boldsymbol{R})\chi_0^+(\boldsymbol{k}_0, \boldsymbol{r}_1)\rangle. \quad (5)$$

Here, $\chi_0^+(\boldsymbol{k}_0, \boldsymbol{r}_1)$ is an initial-state distorted wave obtained with outgoing wave boundary conditions, while $\chi_1^-(\boldsymbol{k}_1, \boldsymbol{r}_1)$ and $\chi_2^-(\boldsymbol{k}_2, \boldsymbol{r}_2)$ are the distorted waves for the scattered and ejected electrons, respectively. Note that these waves are calculated satisfying incoming wave boundary conditions. The factor $C_{12}(\boldsymbol{r}_{12})$ contained in the final state wavefunction is the Coulomb interaction between the two outgoing electrons, which is normally called the postcollision interaction (PCI). Since any physics contained in the wavefunction is automatically contained to all orders of perturbation theory, the M3DW approach contains PCI to all orders of perturbation theory. Finally, $\phi_{Dy}(\boldsymbol{r}_2, \boldsymbol{R})$ is the one-electron Dyson orbital.[32] The TDCSs for the oriented molecule is then obtained from the transition matrix through

$$\frac{d^5\sigma}{d\Omega_1 d\Omega_2 dE}(\boldsymbol{R}) = \frac{1}{(2\pi)^5}\frac{k_1 k_2}{k_0}\left(|T_{dir}(\boldsymbol{R})|^2 + |T_{exc}(\boldsymbol{R})|^2 + |T_{dir}(\boldsymbol{R}) - T_{exc}(\boldsymbol{R})|^2\right). \quad (6)$$

Here, the exchange amplitude, T_{exc}, in Eq. (6) has the same form as the direct scattering amplitude [Eq. (5)], except that the electron coordinates in the final state wavefunction are interchanged. While some experiments have been able to determine cross sections for fixed in space diatomic molecules,[34–38] in the present experiments, the target molecules are randomly oriented in space. Thus, in order to compare the experimental and theoretical results, the TDCSs calculated with the M3DW framework must be averaged over all-possible molecular orientations. In the present work, we perform a proper average (PA), whereby the cross section is calculated over a number of different molecular orientations and then numerically averaged,

$$\frac{d^5\sigma^{PA}}{d\Omega_1 d\Omega_2 dE} = \frac{\int \frac{d^5\sigma}{d\Omega_1 d\Omega_2 dE}(\boldsymbol{R})d\Omega_R}{\int d\Omega_R}. \quad (7)$$

The calculation of the M3DW cross section for a large number of discrete molecular orientations is computationally taxing, particularly for larger molecules. It is therefore desirable to consider approximations that can make such computations more tractable. One possibility is averaging the Dyson orbital, rather that the cross section, over the molecular orientations. In this orientation-averaged molecular orbital (OAMO) approach, the averaged Dyson orbital is expressed through

$$\phi_{Dy}^{OAMO}(\boldsymbol{r}_2) = \frac{\int \phi_{Dy}(\boldsymbol{r}_2, \boldsymbol{R})d\Omega_R}{\int d\Omega_R}. \quad (8)$$

For many molecular states, this average is zero or very small. In such cases, the absolute value of the Dyson orbital is used in calculating the OAMO. The OAMO represents a significant computational saving, as it is equivalent to only calculating the TDCS for a single fixed-in-space molecular orientation. The OAMO method has worked well for a highly symmetric H_2 molecular target,[31] but in other cases, it has been less successful.[22,23,39] Nonetheless, while it has not been good in reproducing the exact details of the TDCS for some molecules, its results can often still provide useful insights into the scattering phenomena.

To assist us in analyzing and interpreting our experimental results, quantum chemical calculations were performed to obtain details on the structure of *R*-carvone. Six possible stable carvone conformers have previously been identified.[40,41] These conformers relate to 3 torsional positions of the isopropenyl group in either equatorial or axial positions with respect to the dihedral angle to the cyclohexene group. They are henceforth denoted by eq-1, eq-2, eq-3, ax-1, ax-2, and ax-3, respectively [see Fig. 1(b)]. Experimental electron diffraction studies have indicated that it is only the eq-1 (62 ± 18%) and eq-2 and eq-3 (combined 38%) conformers that are present in gas-phase experiments.[40] These results are supported by a resonance-enhanced multiphoton ionization investigation, which could also be explained under the assumption that carvone only existed in the three equatorial conformers.[42] Nonetheless, we have performed geometry optimization calculations for the 6 carvone conformers (in both equatorial and axial configurations). These calculations were undertaken within a density functional theory model chemistry employing the Becke three-parameter Lee, Yang, and Parr exchange-correlation functional and an augmented correlation-consistent polarized valence double-zeta basis set (B3LYP/aug-cc-pVDZ).[43,44] Single point energy calculations were also performed at the optimum conformer geometries using the same B3LYP/aug-cc-pVDZ model chemistry in order to determine orbital structural information. Outer-valence Green's function theory calculations with a split valence double-zeta basis with additional polarization functions (OVGF/6-31G*) were also undertaken to obtain the carvone ionization energies (IE). These calculations were performed in the Gaussian 09[45] package. Here, our structural calculations indicate that the carvone conformer populations are 44% equatorial-1, 24% equatorial-2, 29% equatorial-3, and 1% for each axial conformer. This population analysis is consistent with the aforementioned experimental results.[40,41] Given the minor theoretical contributions from the axial conformers (~3%) and the absence of their signatures in the available experimental data, we only consider the three most populated equatorial conformers in our analysis. To assist in the interpretation of the scattering phenomena, spherically averaged momentum profiles of the carvone

Published under license by AIP Publishing

molecular orbitals have been obtained within using the HEMS program.[46] Dyson orbitals for the ionization of carvone were also generated within a target Kohn-Sham approximation, in each of the prominent equatorial conformations for implementation in the M3DW calculations. Within the M3DW framework, the calculation of the TDCSs in the OAMO approximation is insensitive to the R/S chiral inversion. Because the asymmetric coplanar kinematics has symmetry about the scattering plane and the molecular target orientation is random, the TDCS obtained under the current experimental conditions will be identical for both enantiomers, irrespective of the targets chirality. Previously, the total positron scattering cross sections for the R/S enantiomers of methyl-2-chloropropionate, obtained using a partially spin-polarized positron beam, were found to be consistent with each other to within the experimental uncertainties.[47] It is therefore apparent that while our results are for *R*-carvone, they are likely to be equally applicable for the *S*-carvone enantiomer.

III. RESULTS AND DISCUSSION

The observed binding energy spectrum for *R*-carvone is presented in Fig. 2. Photoelectron spectra have been reported previously in Garcia *et al.*[48] using threshold radiation, He(I) and $h\nu$ = 95 eV sources. All of these techniques, and our experimental data, are consistent in that the outermost spectral feature is well separated from the remaining higher-lying valence structure. Our structure calculation derived ionization energies are summarized in Table I, along with the present experimental and corresponding previously reported values. These calculations indicate that the outermost valence feature is composed of the unresolved combination of the three outermost molecular orbitals (41a-39a). Thus, the experimental data and theoretical calculations are consistent in that these three-outermost orbitals are closely lying in energy, with an experimentally observed separation of 0.4 eV.[48] The 41a, 40a, and 39a orbitals relate to the nonbonding oxygen contribution (n_O), and π-bonding contributions associated with the ring and isopropenyl C=C groups. For the three abundant equatorial conformers, the 41a-39a molecular orbitals are illustrated in Fig. 3. While the orbitals may classically be described as a nonbonding oxygen contribution (41a, n_O), and π-bonding contributions associated with the isopropenyl (40a) and ring (39a) C=C bonds, there is still significant mixing of these features, as well as some coupling to the extended carbon ring structure, for all of the equatorial carvone conformers.

The experimentally observed and theoretically calculated angular distributions for the triple differential cross sections for the unresolved outermost valence feature (41a-39a) of *R*-carvone are shown in Fig. 4. Here, the M3DW results either employed the proper

TABLE I. The experimental and theoretical vertical ionization energies (IE) and spectroscopic assignments of *R*-carvone. Also presented are results from a previously reported threshold photoelectron spectra (TPES).[48] See text for further details. (ˆ)—overlapping features.

Experiment			OVGF/6-31G*			TPES[48]	
Feature	Energy (Width)(eV)	Assignment	eq-1 IE (eV)	eq-2 IE (eV)	eq-3 IE (eV)	Energy(eV)	Assignment
I	9.0	41-39a	9.02	9.08	9.00	8.95	41a (n_O)
	(1.5)		8.82	8.83	8.95	9.35ˆ	40a (π)
			9.01	9.01	8.95	9.35ˆ	39a (π)
II	11.4	38-36a	11.24	11.19	11.30	11.55	
	(1.5)		11.42	11.45	11.36		
			11.52	11.57	11.44		
III	12.4	35-34a	12.39	12.28	12.34		
	(1.5)		12.50	12.44	12.54		
IV	13.0	33-32a	12.80	12.87	12.88		
	(1.5)		13.12	13.13	13.13		
V	14.0	31-27a	13.76	13.77	13.78		
	(1.5)		13.92	13.78	13.92		
			14.05	14.07	13.96		
			14.13	14.36	14.25		
			14.39	14.43	14.50		
VI	15.0	26-24a	14.81	14.65	14.67		
	(1.5)		15.24	15.15	15.13		
			15.28	15.32	15.30		
VII	16.6	23-22a	15.82	15.96	15.94		
	(1.5)		16.61	16.66	16.67		
		21a	17.54	17.38	17.42		

Published under license by AIP Publishing

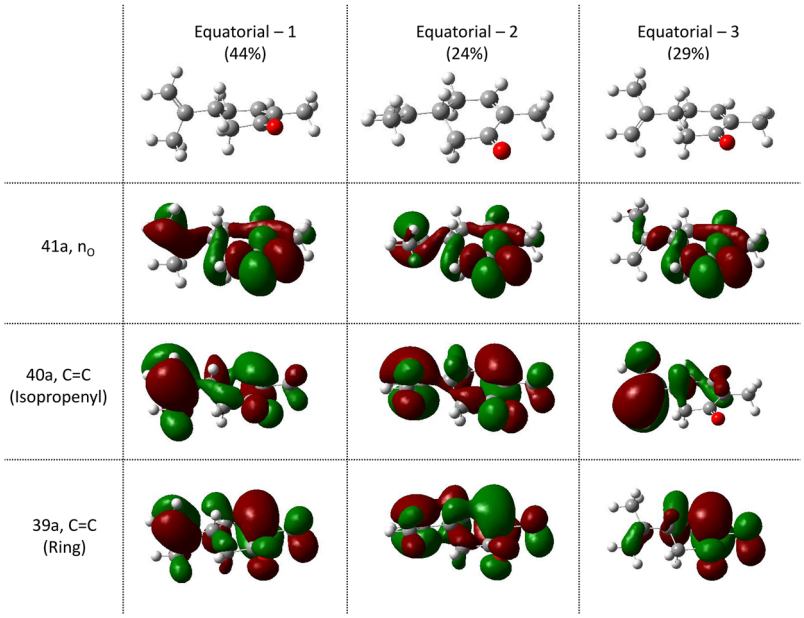

FIG. 3. The 41a, 40a, and 39a molecular orbitals for *R*-carvone in the three equatorial geometries. See text for further details.

averaging or orbital averaging approaches for the population weighted conformer average. In order to compare our theoretical and experimental results, the experimental data have been placed on the absolute scale of the M3DW proper average calculation through a single normalization factor. Here, the normalization factor was determined through a least squares optimization between the experimental and theoretical data for the binary region of the TDCS under the $\theta_1 = -10^\circ$ scattering condition. The proper average M3DW theoretical calculations for each orbital, in each conformer, are presented in Fig. 5. The conformationally averaged TDCS is then obtained by summing the TDCS of each conformer, weighted by its population, 0.44(eq-1) + 0.24(eq-2) + 0.29(eq-3). At the M3DW theoretical level, each molecular orbital gives a TDCS angular distribution where the characteristic behavior does not strongly vary for the different molecular conformations and is therefore largely consistent with the conformationally averaged TDCS. While this is shown explicitly for the proper average results, the same was also true for the M3DW results obtained within the OAMO approximation.

Under each experimental kinematic condition, we observed that the experimental TDCS exhibits substantial intensity at or near the momentum transfer direction. The behavior of the TDCS in this angular region often reflects the nature and importance of postcollision interactions, as well as polarization and exchange effects.[32] Each angular distribution is also similar in that the cross section intensity is typically decreasing as the ejected electron angle moves to angles larger than that corresponding to the momentum transfer direction. In the $\theta_1 = -10^\circ$ and -15° TDCS angular distributions (see Fig. 4), we observe that the cross section intensity is slightly asymmetric about the momentum transfer direction, being slightly larger for the smaller ejected electron angles. The observed angular distribution of the TDCS in the binary region is also in fair agreement with that predicted by the M3DW theoretical calculations employing the proper averaging (PA) approach. Here we note that it is only when the ejected electron angles are smaller than or near to that of the momentum transfer direction that the experimental intensity is somewhat larger than the theoretical prediction. Looking at the magnitude of the cross section under the different scattering kinematics, we observe that the binary region intensity is systematically decreasing as the momentum transfer to the target increases (scattering angle going from $\theta_1 = -5^\circ$ to -15°). This behavior is well-reproduced by the M3DW proper average calculations.

In the recoil region for the fast scattered electron angle of $\theta_1 = -5^\circ$, we do not observe any significant recoil scattering intensity. This observation is qualitatively similar with the M3DW calculations employing the proper average, which does not indicate any significant structures or scattering intensity in the recoil region. We note that we also attempted to measure the TDCS for the $\theta_1 = -10^\circ$ scattering angle condition, but the absence of any recoil scattering intensity led us to abandon the measurements without achieving reasonable statistics for this angular region (data not presented). This is consistent with the TDCS being very small for this kinematic condition, an observation that is confirmed by the M3DW proper average computation.

While the M3DW proper averaging theoretical calculation does a remarkably good job at reproducing the observed scattering behavior, the M3DW calculation that employs an orientation average approximation does a particularly poor job. Here the OAMO approximation produces a TDCS in the binary region that systematically increases in magnitude with increases in the magnitude of the momentum transfer. This behavior is opposite to what occurs experimentally, and also with that predicted using the PA approach. The shape of the binary region TDCS obtained in the OAMO calculations is also inconsistent with the experimental data, with the OAMO TDCS being much narrower in width about the momentum transfer direction. To date, most calculations employing the

Published under license by AIP Publishing

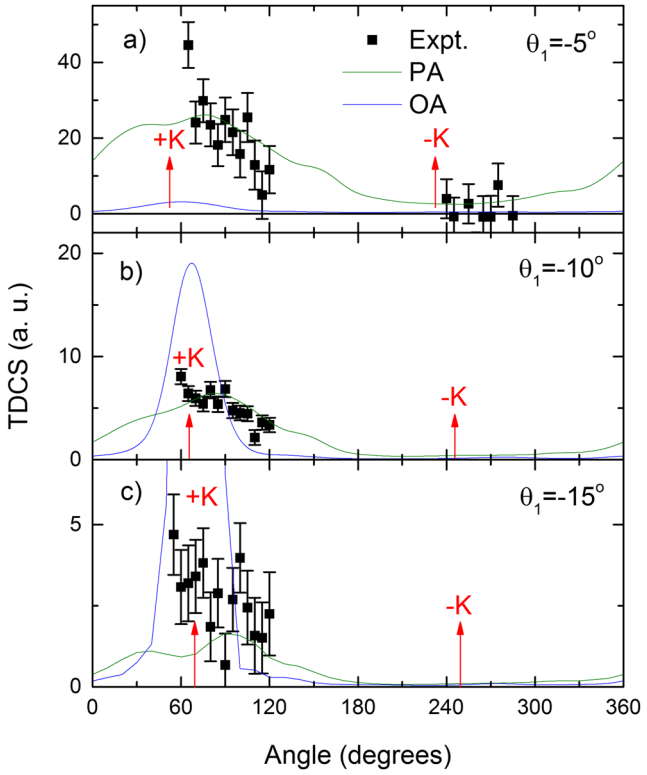

FIG. 4. Experimental and theoretical ejected electron angular distributions of the triple differential cross sections for the electron-impact ionization of the unresolved 41a-39a molecular orbitals of *R*-carvone, for fixed scattered electron angles of (a) −5°, (b) −10°, and (c) −15°. Here, the incident and slow ejected electron energies are fixed at E_0 = 250 eV and E_2 = 20 eV. Theoretical M3DW TDCSs are reported using both the proper average (PA, green) and orientation average (OA, blue) approaches for the carvone conformer-weighted average [0.44(eq-1) + 0.24(eq-2) + 0.29(eq-3)]. Arrows indicate the direction parallel (+K) and anti-parallel (−K) to the momentum transfer direction. See text for further details.

M3DW approach have utilized the OAMO approximation, and have typically been unable to reproduce the experimentally observed phenomenon.[22,23,39] In this instance, where the proper average approach has been implemented for all contributing molecular orbitals, we find remarkably good agreement between the experimental and theoretical results. The significant variation noted here between the OAMO and PA calculations suggests that the phase of the molecular orbital, which is destroyed through the averaging procedure for non-symmetric wave functions, plays an important role in the scattering process. With this in mind, it becomes practicable to identify those orbitals for which we may expect the OAMO approach to breakdown, mandating that the PA approach is employed. As these PA TDCS angular distribution calculations require significant computational resources, if a complete ionization picture is required for all molecular orbitals (such as obtaining a total ionization cross section) it may be reasonable to combine the approaches and specify orbitals for which the PA approach must be employed, and orbitals where the OAMO may still yield reasonable results. The ability to identify molecular orbitals that cannot be described through an OAMO approach, and overcome these limitations through a PA approach represents significant progress in trying to describe the dynamics of the ionization progress in an intermediate energy regime for larger molecules.

As the target's molecular structure information has been qualitatively useful in explaining scattering phenomena previously,[14,19,22,23,49] we have here also calculated spherically averaged orbital momentum profiles for each orbital contributing to the unresolved experimental feature (41a-39a) in each of the abundant equatorial conformers [see Figs. 6(a)–6(c)]. We have also generated a conformer-weighted momentum profile for each molecular orbital, and the sum of these unresolved orbital features [see Fig. 6(d)]. Here we find that the molecular orbitals for the different conformers, while displaying subtle variations, all exhibit characteristic behavior representing the dominant orbital contributions. In particular, the 41a orbital is characteristically non-bonding, displaying p-like contributions from the C/O atoms and an s-like contribution from the extension of the orbital through the carbon frame (giving rise to some intensity at zero momentum). Both the 40a and 39a orbitals display diffuse bonding p-like contributions that arise from the ring and isopropenyl π-bonds. The combined momentum profile for the sum of unresolved orbitals is therefore dominated by the broad p-like profile, but still maintains a substantial contribution at the near zero momentum values.

In the event of a binary collision between the incident and bound electron, with the residual ion acting as a spectator, the recoil ion momentum is equal and opposite to the ejected electron's momentum when it is ionized. This conservation of momentum, within a binary encounter approximation, dictates the accessible regions of the momentum profile that is sampled with the changing of the ejected electron's angle. The accessible regions available for a particular momentum transfer (fast scattered electron angle), in addition to that probed within our experiment, are also shown in Fig. 6(d). While the present experimental conditions do not meet those required to simulate a binary collision between free electrons, this analysis can still provide clues as to how an orbital may qualitatively contribute to the observed scattering phenomena. Here, we find that under the small momentum transfer kinematics, the momentum transfer direction occurs at the momentum profile maximum. As the scattering angle becomes larger, the accessible range of the momentum profile sampled in the collisions increases. In particular, the intensity of the momentum profile, sampled when the ejected electron is detected along the momentum transfer direction (+K), decreases as the scattering angle changes from $\theta_1 = -5°$ to −15°. This behavior is also reflected in the experimental TDCS angular distributions, where we observe that the binary peak intensity decreases with the changing scattered electron angle. In the past, strong correlations between the binary peak behavior and the momentum profile character have been observed for the $\theta_1 = -15°$ TDCS angular distribution, when the momentum transfer vector magnitude matches that of the slow ejected electrons. These correlations have been particularly evident in *para*-benzoquinone[23] and phenol,[22] where the π-bonding networks give rise to a pronounced minimum on the momentum transfer direction. This is due to the orbital momentum profiles of these compounds having no intensity in the s-like, zero momentum, region. In the carvone case, while

Published under license by AIP Publishing

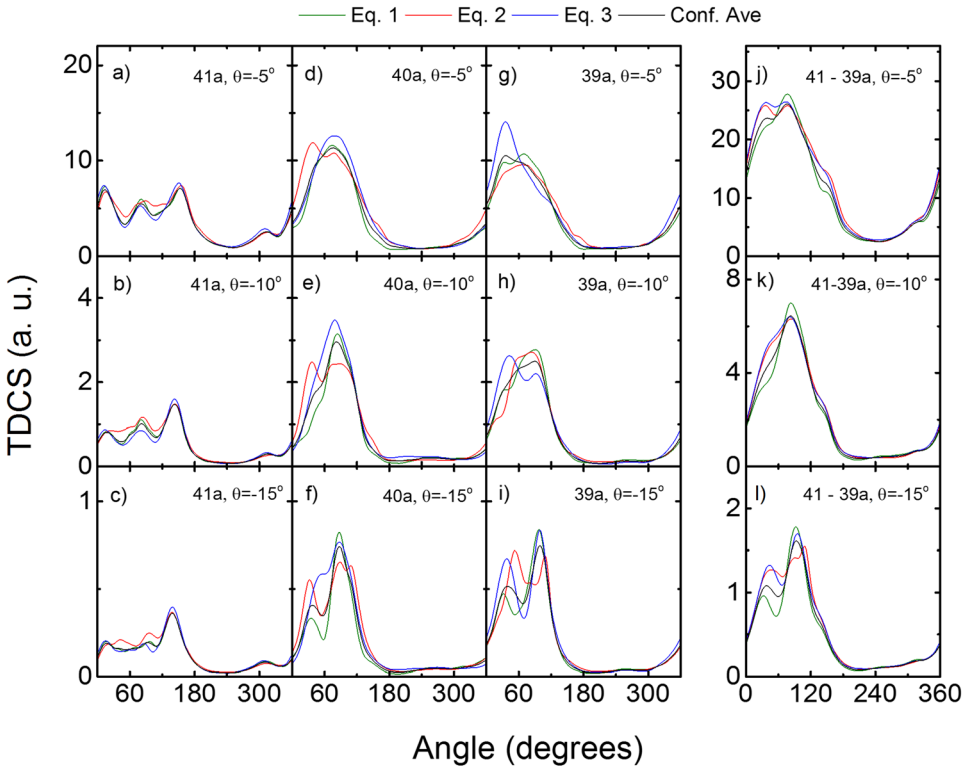

FIG. 5. Proper average (PA) M3DW TDCS (atomic units) angular distributions of a slow ejected electron (E_2 = 20 eV) for the electron impact ionization of the 41a (HOMO) [(a)–(c)], 40a (HOMO-1) [(d)–(f)], 39a (HOMO-2) [(g)–(i)], and unresolved 41a + 40a + 39a [(j)–(l)] molecular orbitals of carvone with the incident electron energy of E_0 = 250 eV, when the scattered electron is detected at −5°, −10°, and −15°, respectively. TDCS are reported for the three abundant equatorial-1 (eq-1, green), equatorial 2 (eq-2, red), equatorial (eq-3, blue) conformers and the population weighted conformer average [0.44(eq-1) + 0.24(eq-2) + 0.29(eq-3), Conf. Ave, black]. See text for further details.

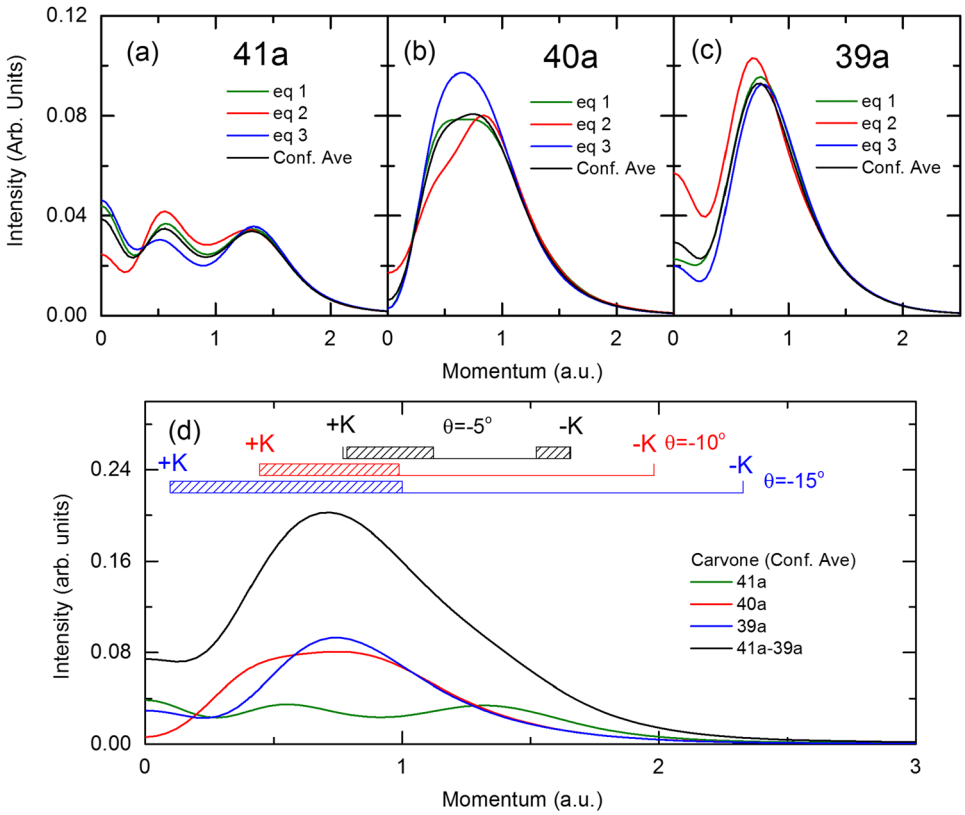

FIG. 6. Theoretical spherically averaged momentum profiles of the (a) 41a, (b) 40a, and (c) 39a molecular orbitals of *R*-carvone in the eq-1, eq-2, and eq-3 conformers. Also shown is the conformer averaged [0.44(eq-1) + 0.24(eq-2) + 0.29(eq-3)] profile. (d) The summed conformationally averaged momentum profiles and each orbitals contribution. Also shown is the range of ion recoil momenta magnitude accessible under the respective scattering conditions for a binary collision in which momentum is conserved. The hatched areas indicate the range examined in the experiments. See text for further details.

Published under license by AIP Publishing

the momentum profiles (Fig. 6) have a characteristic p-dominant shape (π-bonding), the prevalence of the through bond interactions (σ-bonding) gives rise to a s-like contribution of that momentum profile. In this case, there is no minimum in the TDCS angular distribution along the momentum transfer direction (Fig. 4).

The absence of any significant recoil scattering for *R*-carvone is similar to that noted previously in the electron-impact ionization of *para*-benzoquinone[23] and phenol[22] under similar kinematic conditions. In both of those targets, the ionized molecular orbitals belonged to the π-bonding network and nonbonding oxygen (2p) contributions. The absence of any significant recoil scattering was attributed to the diffuse orbital character of the π-bonding and O(2p) orbital contribution that minimizes any of the strong electron-nuclei interactions that are required to generate any significant recoil scattering intensity. The ionization of the unresolved 41a-39a orbitals of carvone is qualitatively similar, in that the ionized orbitals can also be characterized through non-bonding oxygen (n_O) and π-bonding associated with the C=C isopropenyl and ring features. These orbitals are again diffuse, which may contribute to the observed absence of any significant recoil scattering here.

IV. CONCLUSIONS

We have reported an experimental and theoretical investigation into the electron-impact ionization dynamics of *R*-carvone. Theoretical calculations performed at the molecular three-body distorted wave level using a proper averaging approach were able to provide a reasonable reproduction of the experimental data, although some minor differences still existed. When the theoretical calculation used a computationally efficient orientation averaged molecular orbital approximation, the theoretical model produced cross sections whose behavior was in stark contrast to that observed experimentally or with the proper average result. These observations highlighted that the proper averaging approach, for all contributing orbitals, is necessary to qualitatively capture the observed scattering dynamics. Here, the observed scattering phenomena can also be qualitatively explained through the consideration of the target's molecular orbital structure. These results represent significant progress in our efforts to describe ionization dynamics for large molecular targets under an intermediate impact asymmetric energy sharing regime.

ACKNOWLEDGMENTS

This work was partially supported by the Australian Research Council (ARC) through Grant No. DP180101655. E.A. and H.S.C. acknowledge support from the U.S. National Science Foundation Grant No. PHY-1806206. F.F.d.S. acknowledges the Portuguese National Funding Agency FCT-MCTES through researcher position Grant No. IF-FCT IF/00380/2014, and the Research Grant Nos. UID/FIS/00068/2019 (CEFITEC) and PTDC/FIS-AQM/31215/2017. F.F.d.S. also acknowledges Flinders University for a Visiting Researcher Fellowship. M.C.A.L. acknowledges support through a research grant from Brazilian Conselho Nacional de Desenvolvimento Cientifico e Tecnológico (CNPq).

REFERENCES

[1] B. Boudaiffa, P. Cloutier, D. Hunting, M. A. Huels, and L. Sanche, Science **287**, 1658 (2000).
[2] M. J. Brunger, Int. Rev. Phys. Chem. **36**, 333 (2017).
[3] R. D. White, M. J. Brunger, N. A. Garland, R. E. Robson, K. F. Ness, G. Garcia, J. de Urquijo, S. Dujko, and Z. L. Petrović, Eur. Phys. J. D **68**, 125 (2014).
[4] M. J. E. Casey, J. de Urquijo, L. N. Serkovic Loli, D. G. Cocks, G. J. Boyle, D. B. Jones, M. J. Brunger, and R. D. White, J. Chem. Phys. **147**, 195103 (2017).
[5] H. V. Duque, T. P. T. Do, M. C. A. Lopes, D. A. Konovalov, R. D. White, M. J. Brunger, and D. B. Jones, J. Chem. Phys. **142**, 124307 (2015).
[6] J. De Urquijo, M. J. E. Casey, L. N. Serkovic Loli, D. G. Cocks, G. J. Boyle, D. B. Jones, M. J. Brunger, and R. D. White, J. Chem. Phys. **151**, 054309 (2019).
[7] M. J. Brunger, K. Ratnavelu, S. J. Buckman, D. B. Jones, A. Munoz, F. Blanco, and G. García, Eur. Phys. J. D **70**, 46 (2016).
[8] M. C. Fuss, L. Ellis-Gibbings, D. B. Jones, M. J. Brunger, F. Blanco, A. Muñoz, P. Limão-Vieira, and G. García, J. Appl. Phys. **117**, 214701 (2015).
[9] R. D. White, W. Tattersall, G. Boyle, R. E. Robson, S. Dujko, Z. L. Petrovic, A. Bankovic, M. J. Brunger, J. P. Sullivan, S. J. Buckman, and G. Garcia, Appl. Radiat. Isot. **83**(Part B), 77 (2014).
[10] A. I. Lozano, J. C. Oller, D. B. Jones, R. F. da Costa, M. T. do N. Varella, M. H. F. Bettega, F. Ferreira da Silva, P. Limão-Vieira, M. A. P. Lima, R. D. White, M. J. Brunger, F. Blanco, A. Muñoz, and G. Garca, Phys. Chem. Chem. Phys. **20**, 22368 (2018).
[11] A. I. Lozano, K. Krupa, F. Ferreira da Silva, P. Limão-Vieira, F. Blanco, A. Muñoz, D. B. Jones, M. J. Brunger, and G. García, Eur. Phys. J. D **71**, 226 (2017).
[12] M. A. Ridenti, J. Amorim Filho, M. J. Brunger, R. F. da Costa, M. T. do N. Varella, M. H. F. Bettega, and M. A. P. Lima, Eur. Phys. J. D **70**, 161 (2016).
[13] J. D. Builth-Williams, S. M. Bellm, D. B. Jones, H. Chaluvadi, D. H. Madison, C. G. Ning, B. Lohmann, and M. J. Brunger, J. Chem. Phys. **136**, 024304 (2012).
[14] J. D. Builth-Williams, S. M. Bellm, L. Chiari, P. A. Thorn, D. B. Jones, H. Chaluvadi, D. H. Madison, C. G. Ning, B. Lohmann, G. B. da Silva, and M. J. Brunger, J. Chem. Phys. **139**, 034306 (2013).
[15] S. M. Bellm, J. D. Builth-Williams, D. B. Jones, H. Chaluvadi, D. H. Madison, C. G. Ning, F. Wang, X. G. Ma, B. Lohmann, and M. J. Brunger, J. Chem. Phys. **136**, 244301 (2012).
[16] S. M. Bellm, C. J. Colyer, B. Lohmann, and C. Champion, Phys. Rev. A **85**, 022710 (2012).
[17] X. Ren, I. Bray, D. V. Fursa, J. Colgan, M. S. Pindzola, T. Pflüger, A. Senftleben, S. Xu, A. Dorn, and J. Ullrich, Phys. Rev. A **83**, 052711 (2011).
[18] X. Ren, A. Senftleben, T. Pflüger, A. Dorn, K. Bartschat, and J. Ullrich, Phys. Rev. A **83**, 052714 (2011).
[19] D. B. Jones, J. D. Builth-Williams, S. M. Bellm, L. Chiari, H. Chaluvadi, D. H. Madison, C. G. Ning, B. Lohmann, O. Ingolfsson, and M. J. Brunger, Chem. Phys. Lett. **572**, 32 (2013).
[20] C. J. Colyer, S. M. Bellm, B. Lohmann, G. F. Hanne, O. Al-Hagan, D. H. Madison, and C. G. Ning, J. Chem. Phys. **133**, 124302 (2010).
[21] J. D. Builth-Williams, G. B. da Silva, L. Chiari, D. B. Jones, H. Chaluvadi, D. H. Madison, and M. J. Brunger, J. Chem. Phys. **140**, 214312 (2014).
[22] G. B. da Silva, R. F. C. Neves, L. Chiari, D. B. Jones, E. Ali, D. H. Madison, C. G. Ning, K. L. Nixon, M. C. A. Lopes, and M. J. Brunger, J. Chem. Phys. **141**, 124307 (2014).
[23] D. B. Jones, E. Ali, C. G. Ning, J. Colgan, O. Ingólfsson, D. H. Madison, and M. J. Brunger, J. Chem. Phys. **145**, 164306 (2016).
[24] C. C. C. R. de Carvalho and M. M. R. da Fonseca, Food Chem. **95**, 413 (2006).
[25] M. L. da Rocha, L. E. G. Oliveira, C. C. M. Patrício Santos, D. P. de Sousa, R. N. de Almeida, and D. A. M. Araújo, J. Nat. Med. **67**, 743 (2013).
[26] A. G. Sanz, M. C. Fuss, A. Munoz, F. Blanco, P. Limao-Vieira, M. J. Brunger, S. J. Buckman, and G. Garcia, Int. J. Radiat. Biol. **88**, 71 (2012).
[27] M. C. Fuss, A. G. Sanz, A. Muñoz, F. Blanco, M. J. Brunger, S. J. Buckman, P. Limão-Vieira, and G. García, Appl. Radiat. Isot. **83**(Part B), 159 (2014).
[28] F. Blanco, A. Muñoz, D. Almeida, F. Ferreira da Silva, P. Limão-Vieira, M. C. Fuss, A. G. Sanz, and G. García, Eur. Phys. J. D **67**, 199 (2013).

Published under license by AIP Publishing

[29]R. E. Robson, M. J. Brunger, S. J. Buckman, G. Garcia, Z. L. Petrović, and R. D. White, Sci. Rep. **5**, 12674 (2015).
[30]S. J. Cavanagh and B. Lohmann, J. Phys. B: At., Mol. Opt. Phys. **32**, L261 (1999).
[31]J. Gao, J. L. Peacher, and D. H. Madison, J. Chem. Phys. **123**, 204302 (2005).
[32]D. H. Madison and O. Al-Hagan, J. At., Mol., Opt. Phys. **2010**, 367180.
[33]E. Ali, K. Nixon, A. Murray, C. Ning, J. Colgan, and D. Madison, Phys. Rev. A **92**, 042711 (2015).
[34]D. B. Jones, M. Yamazaki, N. Watanabe, and M. Takahashi, Phys. Rev. A **87**, 027714 (2013).
[35]E. Ali, X. Ren, A. Dorn, C. Ning, and D. Madison, J. Phys. B: At., Mol. Opt. Phys. **48**, 115201 (2015).
[36]M. Takahashi, N. Watanabe, Y. Khajuria, Y. Udagawa, and J. H. D. Eland, Phys. Rev. Lett. **94**, 213202 (2005).
[37]E. Ali, A. L. Harris, J. Lower, E. Weigold, C. G. Ning, and D. H. Madison, Phys. Rev. A **89**, 062713 (2014).
[38]S. Bellm, J. Lower, E. Weigold, and D. W. Mueller, Phys. Rev. Lett. **104**, 023202 (2010).
[39]D. B. Jones, E. Ali, K. L. Nixon, P. Limão-Vieira, M.-J. Hubin-Franskin, J. Delwiche, C. G. Ning, J. Colgan, A. J. Murray, D. H. Madison, and M. J. Brunger, J. Chem. Phys. **143**, 184310 (2015).
[40]T. Egawa, Y. Kachi, T. Takeshima, H. Takeuchi, and S. Konaka, J. Mol. Struct. **658**, 241 (2003).
[41]J. Lambert, R. N. Compton, and T. D. Crawford, J. Chem. Phys. **136**, 114512 (2012).
[42]M. Mineyama and T. Egawa, J. Mol. Struct. **734**, 61 (2005).
[43]C. Lee, W. Yang, and R. G. Parr, Phys. Rev. B **37**, 785 (1988).
[44]T. H. Dunning, J. Chem. Phys. **90**, 1007 (1989).
[45]M. J. Frisch, G. W. Trucks, H. B. Schlegel, G. E. Scuseria, M. A. Robb, J. R. Cheeseman, G. Scalmani, V. Barone, B. Mennucci, G. A. Petersson, H. Nakatsuji, M. Caricato, X. Li, H. P. Hratchian, A. F. Izmaylov, J. Bloino, G. Zheng, J. L. Sonnenberg, M. Hada, M. Ehara, K. Toyota, R. Fukuda, J. Hasegawa, M. Ishida, T. Nakajima, Y. Honda, O. Kitao, H. Nakai, T. Vreven, J. A. Montgomery, J. E. Peralta, F. Ogliaro, M. Bearpark, J. J. Heyd, E. Brothers, K. N. Kudin, V. N. Staroverov, R. Kobayashi, J. Normand, K. Raghavachari, A. Rendell, J. C. Burant, S. S. Iyengar, J. Tomasi, M. Cossi, N. Rega, J. M. Millam, M. Klene, J. E. Knox, J. B. Cross, V. Bakken, C. Adamo, J. Jaramillo, R. Gomperts, R. E. Stratmann, O. Yazyev, A. J. Austin, R. Cammi, C. Pomelli, J. W. Ochterski, R. L. Martin, K. Morokuma, V. G. Zakrzewski, G. A. Voth, P. Salvador, J. J. Dannenberg, S. Dapprich, A. D. Daniels, Ö. Farkas, J. B. Foresman, J. V. Ortiz, J. Cioslowski, and D. J. Fox, GAUSSIAN 09, Revision B.01, Gaussian, Inc., Wallingford, CT, 2010.
[46]J. P. D. Cook and C. E. Brion, Chem. Phys. **69**, 339 (1982).
[47]L. Chiari, A. Zecca, S. Girardi, A. Defant, F. Wang, X. G. Ma, M. V. Perkins, and M. J. Brunger, Phys. Rev. A **85**, 052711 (2012).
[48]G. A. Garcia, L. Nahon, and I. Powis, Int. J. Mass Spectrom. **225**, 261 (2003).
[49]S. Xu, X. Ma, S. Yan, and P. Zhang, J. Chem. Phys. **136**, 237101 (2012).

Published under license by AIP Publishing